AD-A236 345

AL-TR-90-070 AD:

Final Report
for the period
January 1989 to
February 1991

SIMULATING THE VORTEX IN A SPINNING ROCKET

May 1991

Author:
A.S. Knappenberger

DTIC
ELECTE
MAY 3 1 1991
S B D

91-00645

Phillips Laboratory

Air Force Systems Command
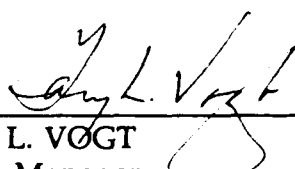Propulsion Directorate
Edwards AFB CA 93523-5000

91

NOTICE

When U.S. Government drawings, specifications, or other data are used for any purpose other than a definitely related Government procurement operation, the fact that the Government may have formulated, furnished, or in any way supplied the said drawings, specifications, or other data, is not to be regarded by implication or otherwise, or in any way licensing the holder or any person or corporation, or conveying any rights or permission to manufacture, use, or sell any patented invention that may be regarded thereto.
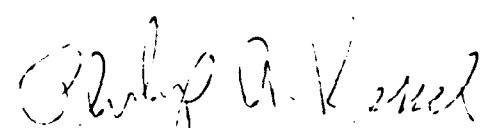
FOREWORD

This final report was submitted by Anjanette Knappenberger on completion of a cold flow experimental investigation of coning forces in spin-stabilized systems at the OL-AC Phillips Laboratory (AFSC), Edwards Air Force Base, CA. PL Project Manager was Gary L. Vogt.

This report has been reviewed and is approved for release and distribution in accordance with the distribution statement on the cover and on the DD Form 1473.

GARY L. VOGT
Project Manager

PHILIP A. KESSEL
Chief, Thermophysics Branch

DAVID W. LEWIS, MAJOR, USAF
Acting Director
Fundamental Technologies Division

REPORT DOCUMENTATION PAGE

Form Approved
OMB No 0704-0188

1a REPORT SECURITY CLASSIFICATION	1b RESTRICTIVE MARKINGS
UNCLASSIFIED	N/A

2a SECURITY CLASSIFICATION AUTHORITY	3 DISTRIBUTION/AVAILABILITY OF REPORT
2b DECLASSIFICATION/DOWNGRADING SCHEDULE	Approved for Public Release. Distribution is unlimited.

4 PERFORMING ORGANIZATION REPORT NUMBER(S)	5 MONITORING ORGANIZATION REPORT NUMBER(S)
AL-TR-90-070	

6a NAME OF PERFORMING ORGANIZATION	6b OFFICE SYMBOL (If applicable)	7a NAME OF MONITORING ORGANIZATION
Phillips Laboratory (AFSC)		

6c. ADDRESS (City, State, and ZIP Code)	7b ADDRESS (City, State, and ZIP Code)
OL-AC PL/RKFT Edwards AFB, CA 93523-5000	

8a NAME OF FUNDING/SPONSORING ORGANIZATION	8b OFFICE SYMBOL (If applicable)	9 PROCUREMENT INSTRUMENT IDENTIFICATION NUMBER

8c ADDRESS (City, State, and ZIP Code)	10 SOURCE OF FUNDING NUMBERS

	PROGRAM ELEMENT NO	PROJECT NO	TASK NO	WORK UNIT ACCESSION NO
	5730	00	A5	

11 TITLE (Include Security Classification)

SIMULATING THE VORTEX IN A SPINNING ROCKET

12 PERSONAL AUTHOR(S)
Knappenberger, A.S.

13a TYPE OF REPORT	13b TIME COVERED	14. DATE OF REPORT (Year, Month, Day)	15 PAGE COUNT
Final	FROM 8901 TO 9102	9105	48

16 SUPPLEMENTARY NOTATION

17	COSATI CODES		18 SUBJECT TERMS (Continue on reverse if necessary and identify by block number)
FIELD	GROUP	SUB-GROUP	Spinning Rockets, Spin Stabilized, Internal Ballistics Nutation Instability, Axial Vortex, Flow, Gasdynamic Driving, Jet Damping, Gas Sloshing.
21	08	2	

19 ABSTRACT (Continue on reverse if necessary and identify by block number)

The continuing phenomena of coning in spin stabilized motor/spacecraft is investigated using a laboratory-scale vortex generating model. This model simulated some of the forces associated with a vortex flow and allowed for altering the relationship between the vortex core flow and the nozzle. Altering the vortex core centerline produced differences in the measured side forces. The first configuration, with the vortex center aligned with the nozzle, produced no disturbing side forces. In subsequent tests, the misalignment of the vortex centerline with the nozzle centerline produced a side force that deflected the model from the vertical reference. The tangential velocity of the forced vortex produced the disturbing moment on the model. The forced acted on the through a line perpendicular to a line between the vortex center and the nozzle centerline. Momentum theory accurately predicted the disturbing side forces.

20 DISTRIBUTION/AVAILABILITY OF ABSTRACT	21. ABSTRACT SECURITY CLASSIFICATION
[X] UNCLASSIFIED/UNLIMITED ☐ SAME AS RPT ☐ DTIC USERS	UNCLASSIFIED

22a NAME OF RESPONSIBLE INDIVIDUAL	22b TELEPHONE (Include Area Code)	22c OFFICE SYMBOL
Gary L. Vogt	805-275-5258	OL-AC PL/RKFT

DD Form 1473, JUN 86 — Previous editions are obsolete — SECURITY CLASSIFICATION OF THIS PAGE

TABLE OF CONTENTS

FIGURES

NOMENCLATURE

A	flow cross sectional area
a	speed of sound
α	deflection angle
F_S	side force
γ	specific heat ratio
h	height of vortex chamber
h_{eff}	effective height of vortex chamber
M	Mach number
m	mass flow rate
P_S	static pressure
P_T	total pressure
R	gas constant
ρ	density
T_S	static temperature
T_T	total temperature
V	velocity
W	weight of the model
w	diameter of the nozzle

INTRODUCTION

During orbit transfer operations using spin stabilized motor/spacecraft, a nutational instability, referred to in this report and others as "coning" or "wobbling," caused the spacecraft to enter an orbit with its spin axis nutating about its flight path. This phenomenon manifests itself as a growing precession of the primary spin axis about the flight path thus cutting the shape of a cone. Final coning angle has reached a maximum of 17 degrees and averaged 10 degrees before the routine application of nutation control systems (NCS). Investigation of over 22 theories and mechanisms have added some knowledge to the understanding of coning. Still, there is no definitive mechanism to which coning may be attributed.

Spinning a solid propellant motor and spacecraft configuration for stabilization during orbit transfer has the advantage of inherent low cost and simplicity. Currently the only solution to the coning problem is the addition of an NCS. These additional attitude control packages add complexity and increase development and operational costs. In addition, the NCS adversely affects the payload capability of the spinning rocket due to the increased weight. A better approach would be isolating the cause of the problem and understanding the mechanism responsible for coning.

The combustion gases and products, which flow from the edge of the propellant towards the center line of the rocket nozzle, increasingly travel a greater distance and are more subject to external forces as the solid propellant burns. These additional forces are not accounted for in classical jet damping or when using one or two dimensional models in a spinning environment. When the vortex center line deviates from the nozzle center line then, according to the theory tested in this report, the resulting moment creates a side force which acts on the nozzle. The design of the experimental model allows for placing the center of the vortex at increasing radial distances from the nozzle center. Any resulting disturbing force results in a deflection of the model. The plexiglass model also provided a visual investigation of the vortex.

APPARATUS

The model, designed to simulate the vortex motion inside a spinning rocket by forced injection rather than spin, consists of five plexiglass pieces assembled to form a 101.6x101.6x76.2 millimeter (mm) cube, Figure 1. A flexible hose suspended the model and acted as a pivot point and allowed for unrestricted movement of the model. Pressurized nitrogen passed through the flexible hose to a stainless steel tube attached to the model. The nitrogen enters an area surrounded on the outside by a 101.6x101.6x25.4 mm spacer. The spacer, placed in this void, contains a 71 mm diameter cavity for one of two inserts. The inserts use a set of four injectors, each 3.18 mm in diameter, that inject the nitrogen into an inner chamber measuring 10.16 mm in height and 30.48 mm in diameter.

Two different inserts were tested: one experimental and one as a control. The experimental insert used tangential injectors, thus creating a forced vortex in the insert chamber. In the control insert, the injectors are aligned perpendicular to the

chamber wall on a radial line to the center. The 101.6x101.6x25.4 (mm) bottom piece contained a nozzle through the center which allowed the nitrogen to escape. Figure 2 shows the assembled configuration.

Flexible
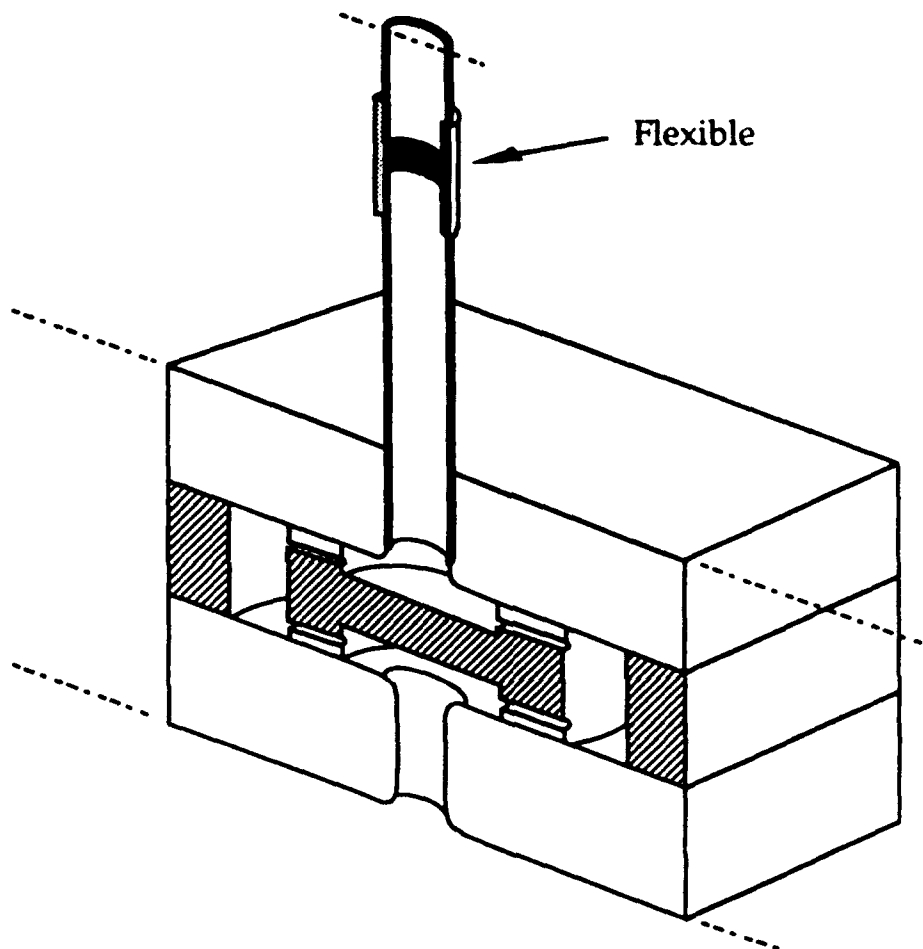
FIGURE 1 ISOMETRIC SECTION OF THE VORTEX MODEL

As the schematic of Figure 3 shows, a pressure gauge measured the total and static pressure in the vortex chamber. A rotameter and a pressure gauge regulated the nitrogen pressure and the mass flow rate through the model.

Modifications to the model tested several possible configurations. An additional spacer created a taller vortex chamber (Figure 4a) in the first modification. This configuration included a small plexiglass tube, 25.4 mm high and having an outer diameter of 20.65 mm and an inner diameter equal to the nozzle (Figure 4b), placed directly above the nozzle. This configuration determined if recirculation areas surrounding the nozzle tube affected the behavior of the model. Another configuration included the extra spacer but not the nozzle tube. Clay, placed in the lower half of the vortex chamber, formed a smooth transition from the edge of the chamber to the nozzle entrance (Figure 4c).

Spacer

Tangential Injectors Of The
Experimental Insert

Injector Insert

Injector

A

A

Nozzle

Section through A-A
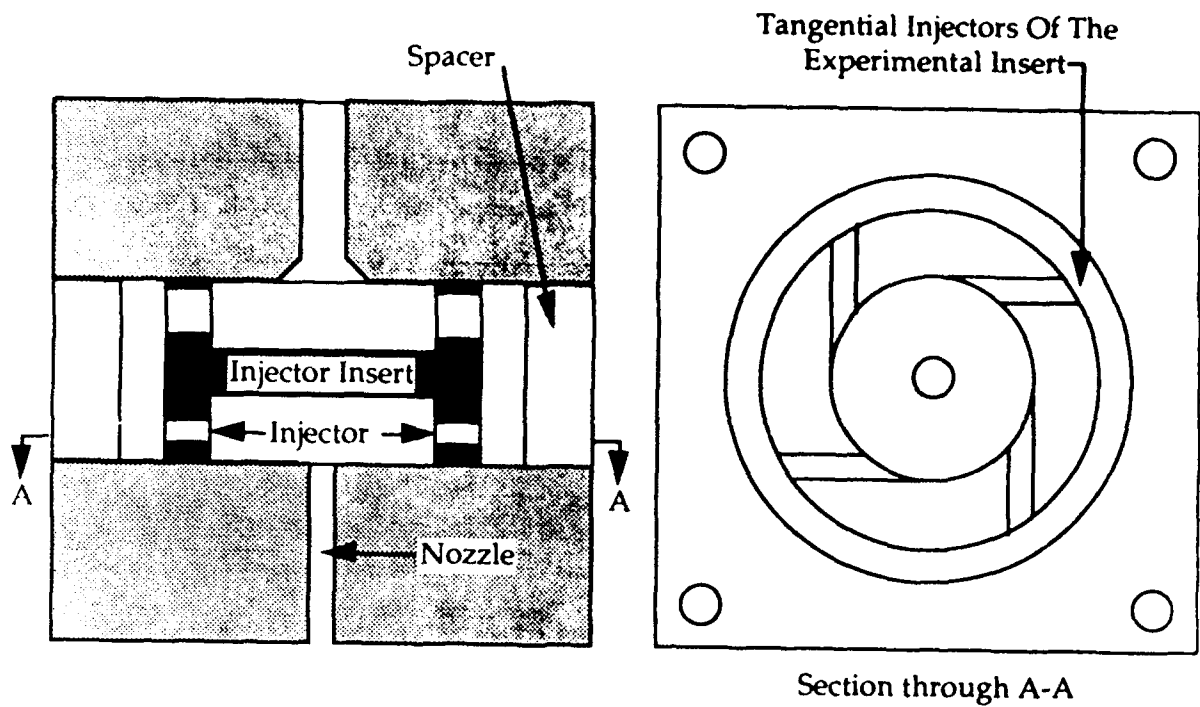
FIGURE 2

VORTEX MODEL DETAILS

Control
Valve

Nitrogen
Source

Total Pressure
Measurement
For Flow Rate
Calculation

Pitot Pressure
Measurement

Exhaust Gas
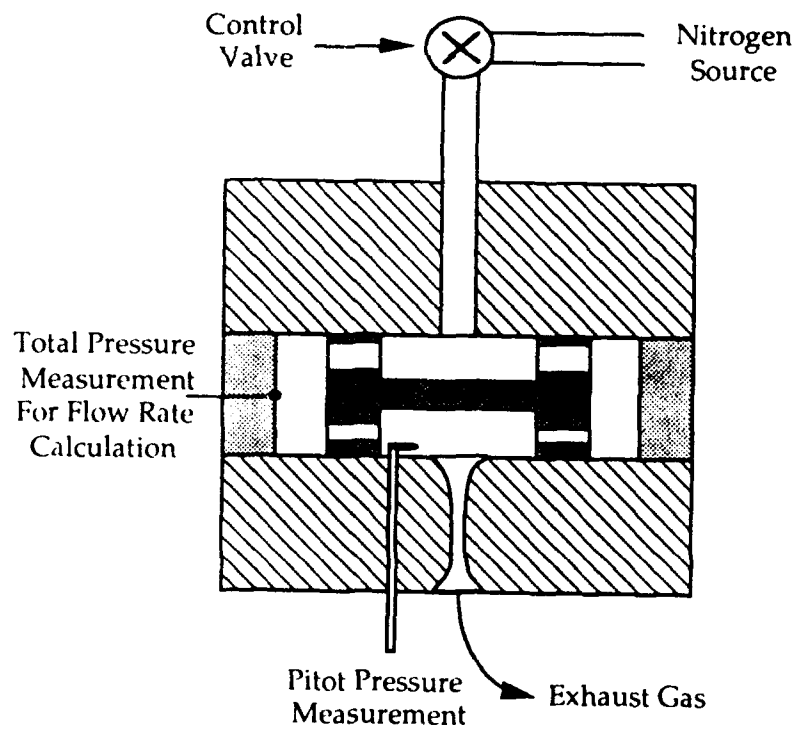
FIGURE 3

SCHEMATIC OF THE VORTEX MODEL

4

Insert Extension

Additional Spacer
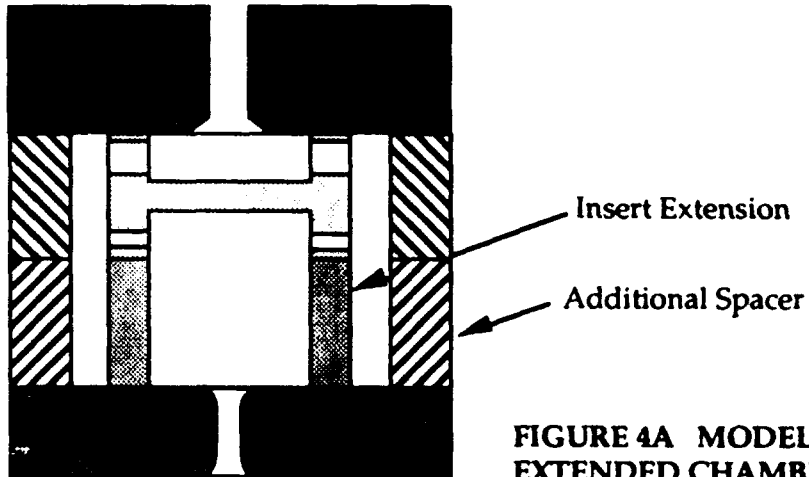
FIGURE 4A MODEL WITH EXTENDED CHAMBER
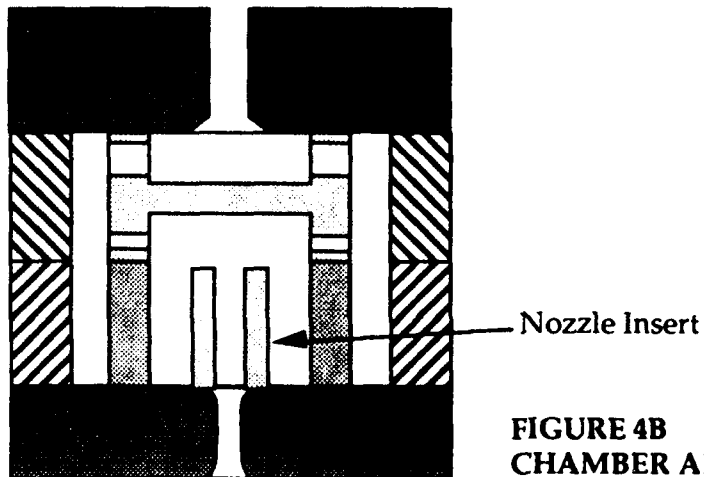
Nozzle Insert

FIGURE 4B MODEL WITH EXTENDED CHAMBER AND NOZZLE INSERT
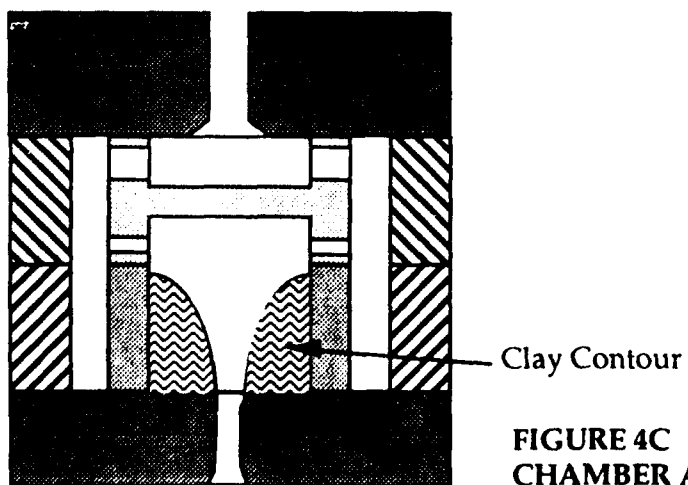
Clay Contour

FIGURE 4C MODEL WITH EXTENDED CHAMBER AND CLAY CONTOURING

FIGURE 4 ADDITIONAL VORTEX MODEL EXPERIMENT CONFIGURATIONS

TEST DESCRIPTION

Figure 5 shows a series of holes in the bottom piece which in the assembled model opened into the vortex chamber. The holes allow for insertion of a pitot tube, Figure 6, to measure the total and static pressures in a cross section of the chamber. The total and static pressures were measured by adjusting the length and position of the pitot tube for several test runs. Comparisons between the measured side force of the original vortex model and the measured side forces of the modified model appear in Figure 7.

Preliminary differential pressure measurements between the insert entrance and chamber (the exit of the injectors) verified and insured choked flow through the injectors.

The insert design allowed for various off-sets of the chamber centerline from the nozzle centerline. Initial test runs verified the behavior of the model with the insert centerline aligned with the nozzle centerline. The off-center placement of the insert in following tests demonstrated the side forces produced by an off-set forced vortex. The insert off-set distance and the resulting measured side forces are shown in Figure's 8-19.

Holes for Pitot Tube Pressure Measurements

FIGURE 5

VORTEX MODEL BASE IN DETAIL

6

Total Pressure
Pitot Tube

Static Pressure
Pitot Tube

4 0.015 Dia
Holes

0.125 In

Total Pressure Pitot
Tube

Static Pressure Pitot Tube

0.063 In

0.063 In

FIGURE 6

DETAILS OF THE PITOT TUBE

Appendix A is a record of these measurements as a function of the radial distance from the nozzle center and the height above the entra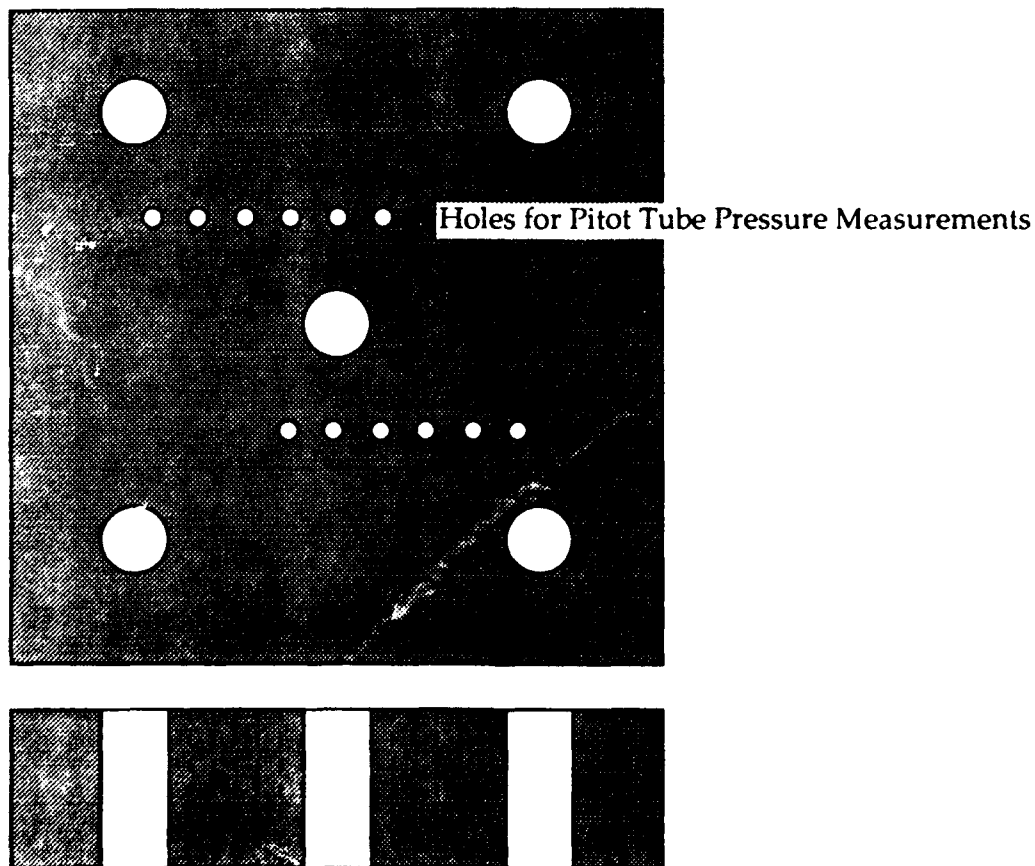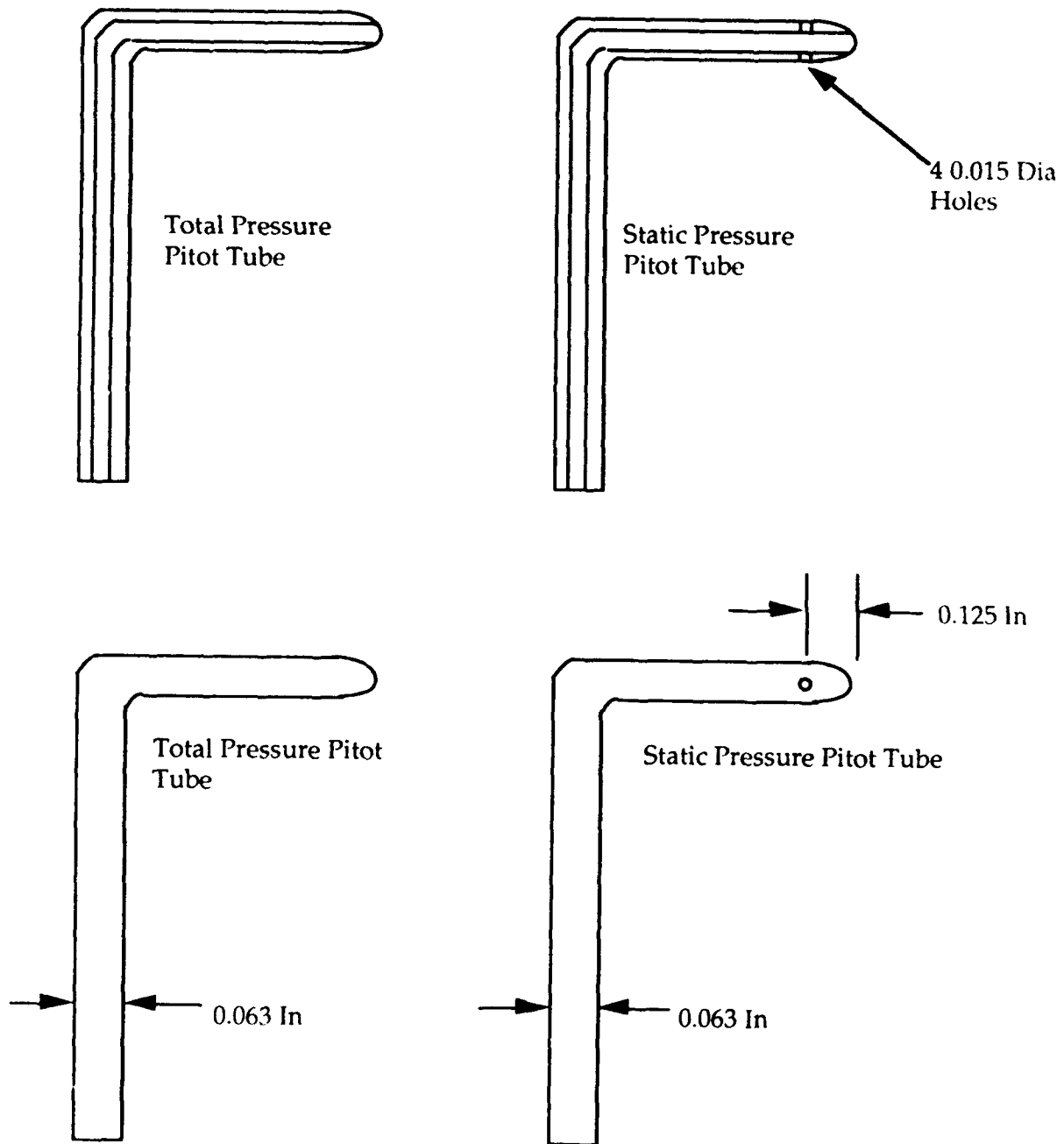nce to the nozzle. The mean and standard deviation at each insert position also appear in Appendix A and are the basis for further calculations. Appendix B includes information on the deflection amplitude relative to a stationary reference for each insert position which exhibited a disturbing side force.

EXPERIMENTAL RESULTS

Initial base-line tests using the control insert (perpendicular injectors) did not produce any sort of a model deflection from the vertical, regardless of the position of the insert. Initial tests with the experimental (tangential injectors) insert aligned with the center of the nozzle also produced no disturbing side forces. However, when the experimental insert centerline was off-set from the nozzle centerline, a deflection of the model occurred. The deflection magnitude varied with the misalignment of the insert and the model remained in that position until the nitrogen flow stopped.

As the insert position moved further from the nozzle center line, the nitrogen flow through the injectors may no longer be uniform. To examine a worst case scenario, an insert with a sealed injector was tested to determine how this would affect the force on the model. The results indicate that if a restricted flow through one of the injectors causes a disturbing force, the force is insignificant in comparison to the force produced by the misaligned vortex.

The apparent force produced by the vortex flow acts perpendicular to the center line of the nozzle and in a direction dictated by the tangential velocity. The magnitude of the side force is:

$$F_S = W \tan \alpha \tag{1}$$

where F_S is the side force and α is the deflection angle.

The modified model with an extended vortex chamber placed off-center again produced a deflection. The force required to produce this deflection is slightly less than for the original model. For example, with the center of the vortex and the center of the nozzle of both configurations displaced to their maximum off-set, 4.83 mm, the measured side force of the original model (0.26 Newtons) is 0.02 Newtons greater than for the modified model (0.24 Newtons).

In a second configuration, the addition of a nozzle tube created recirculation areas on the lower outer edge of the off-center extended vortex chamber. With the centers displaced by 4.83 mm, the resulting side force is 0.21 Newtons. This value is 0.05 Newtons less than the model without the nozzle tube.

In another configuration, clay formed a smooth transition in the lower half of the extended vortex chamber from the inner wall to the nozzle entrance. The results of this configuration with displaced centers were similar to those of previous tests: a force of 0.09 Newtons.
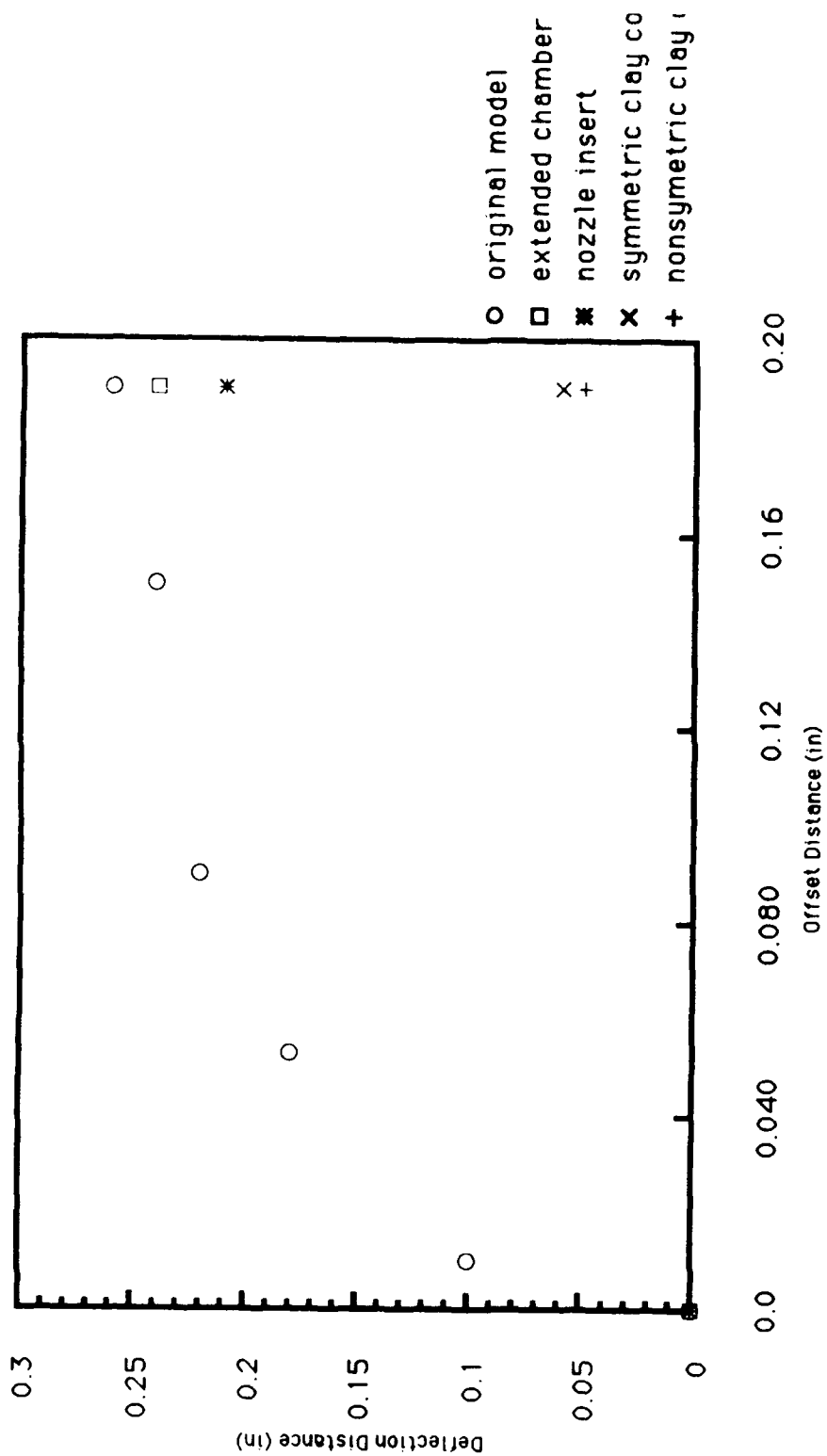
Legend:
- ○ original model
- □ extended chamber
- ✻ nozzle insert
- ✕ symmetric clay co
- + nonsymmetric clay

Figure 7
Measured Deflection of the Vortex Model Configurations

THEORETICAL RESULTS

A comparison of the observed disturbing side force to a calculated side force will test the misalignment theory. The first step is a calculation of the velocity at the nozzle entrance. The Mach number, calculated by using the mean total and static pressures taken at the center of the nozzle and assuming steady flow and one dimensional isentropic ideal gas behavior, is:

$$\frac{P_T}{P_S} = \left[1 + \frac{\gamma - 1}{2} M^2 \right]^{\frac{\gamma}{\gamma - 1}} \tag{2}$$

where P_T is the total pressure and P_S is the static pressure. Rearrangement leads to:

$$M = \left[\frac{2 \left(\frac{P_T}{P_S} \right)^{\frac{\gamma - 1}{\gamma}} - 2}{\gamma - 1} \right]^{\frac{1}{2}} \tag{3}$$

For a total temperature assumed equal to a room temperature of 294.1 degrees Kelvin (21.1° C), the static temperature is:

$$T_S = \frac{T_T}{1 + \frac{\gamma - 1}{2} M^2} \tag{4}$$

From the calculated Mach number and the static temperature, the velocity is:

$$a = \sqrt{\gamma R T} \tag{5}$$

and

$$V = Ma \tag{6}$$

Figures 8-13 show the relationship of the total and static pressures. Figures 14-19 are the resulting velocity profiles. In the velocity profiles, the velocity reference is positive on one side of the nozzle and negative on the opposing side.

The density of the gas flow is:

$$\rho = \left(\frac{P_T}{RT_T} \right) \left(\frac{P_S}{P_S} \right)^{\gamma^1} \tag{7}$$

The product of the measured volumetric flow rate, obtained from the rotameter, and the density yields the mass flow rate.

The observed direction of the deflection force, coincident with the tangential gas velocity at the nozzle, suggested that the side force behaved as if the flow were directed into the nozzle by an imaginary duct, Figure 20.
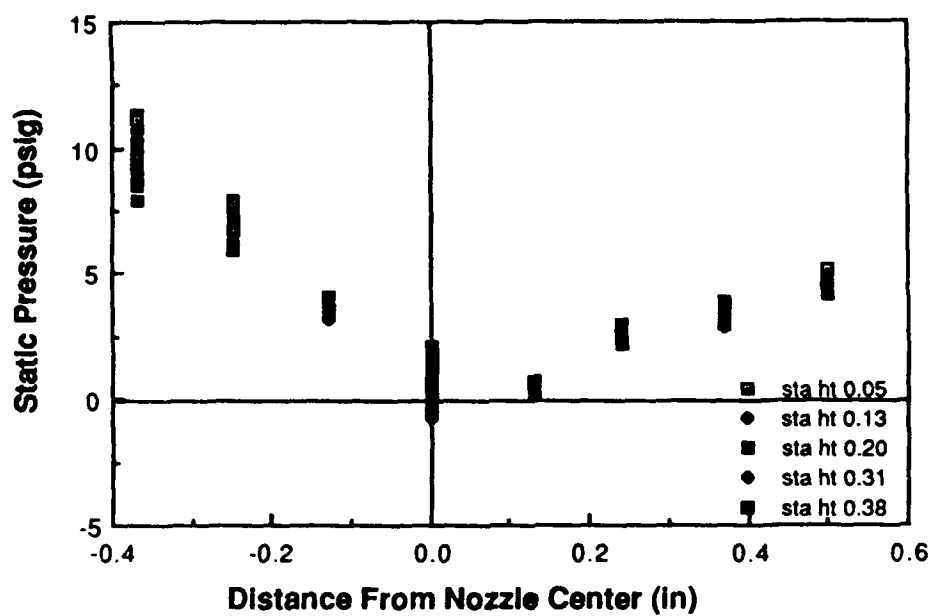
Figure 8a Static Pressure Versus the Radial Distance
Coincident Centers
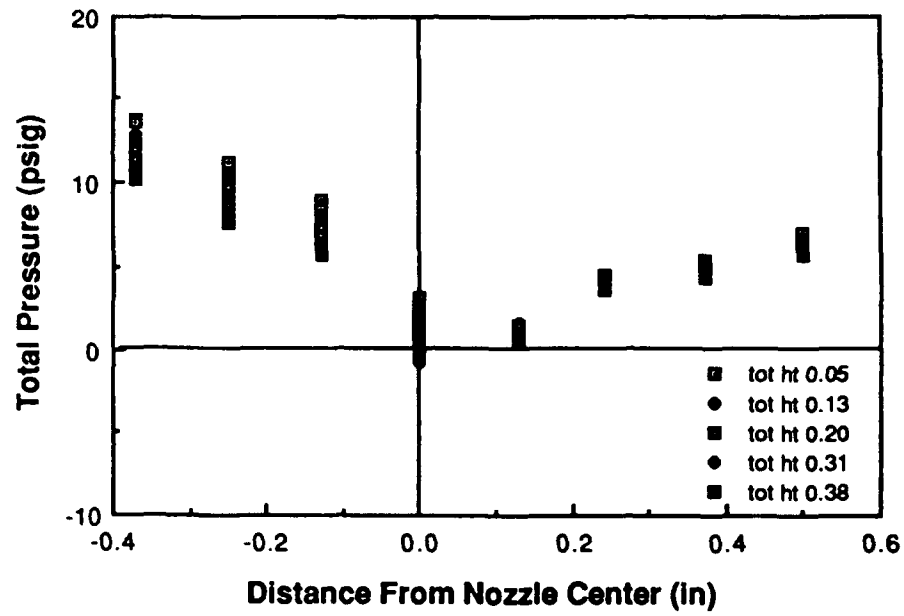
Figure 8b Total Pressure Versus the Radial Distance
Coincident Centers

Figure 9a Static Pressure Versus the Radial Distance

Offset of 0.210 in

Figure 9b Total Pressure Versus the Radial Distance
Offset of 0.250 in

Figure 10a Static Pressure Versus the Radial Distance
Offset of 0.250 in

Figure 10b Total Pressure Versus the Radial Distance
Offset of 0.250 In
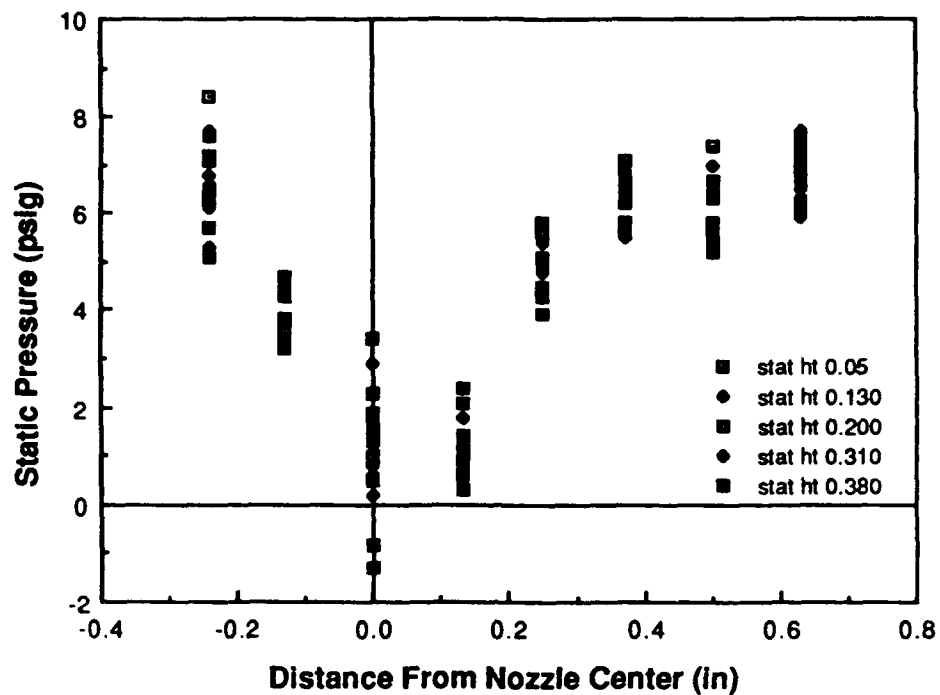
Figure 11a Static Pressure Versus the Radial Distance
Offset of 0.300 in
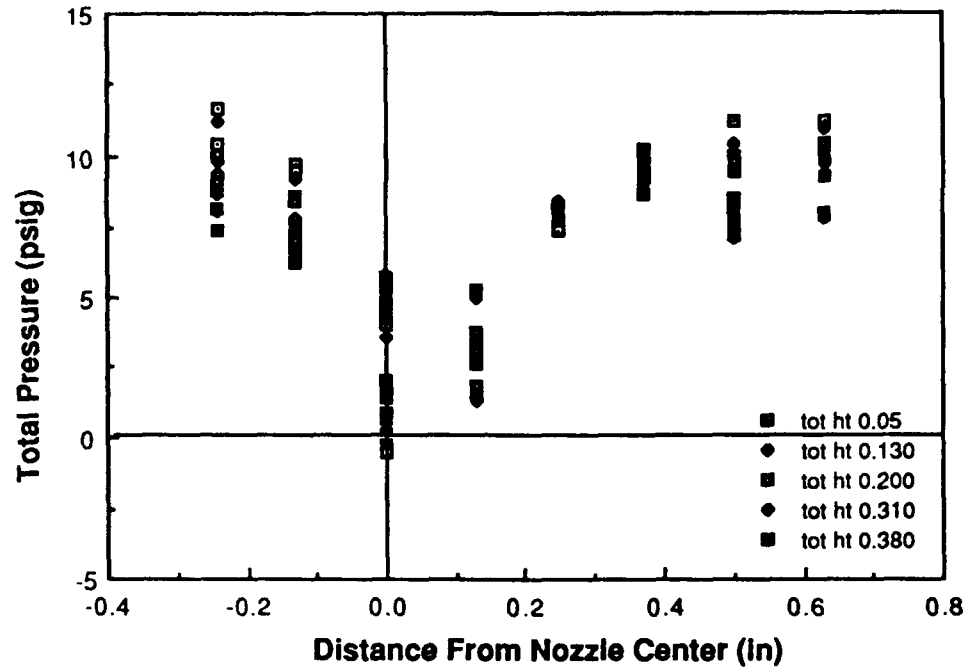
Figure 11b Total Pressure Versus the Radial Distance
Offset of 0.300 in
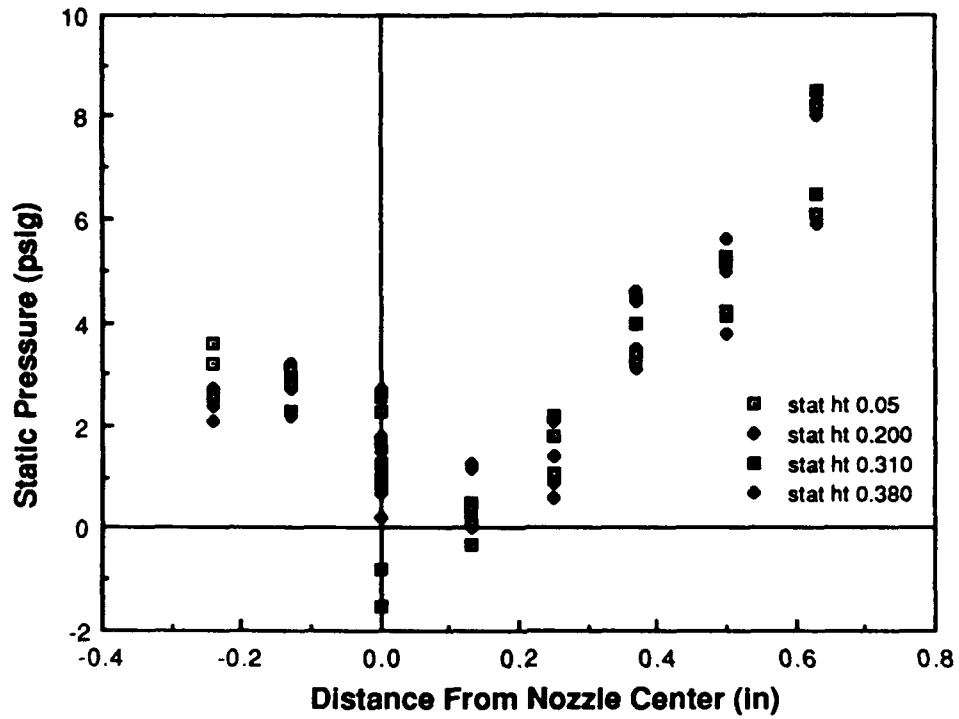
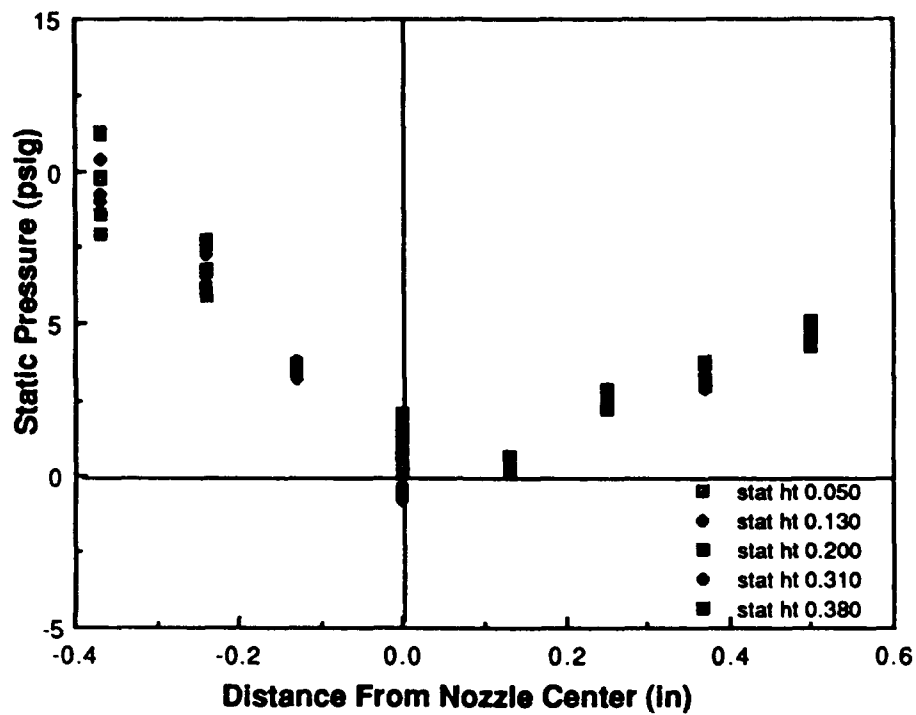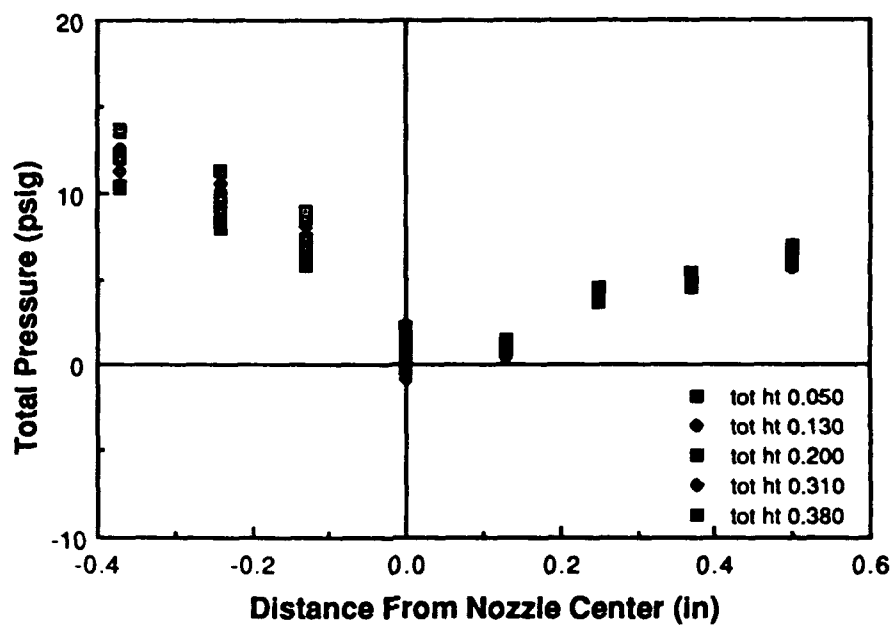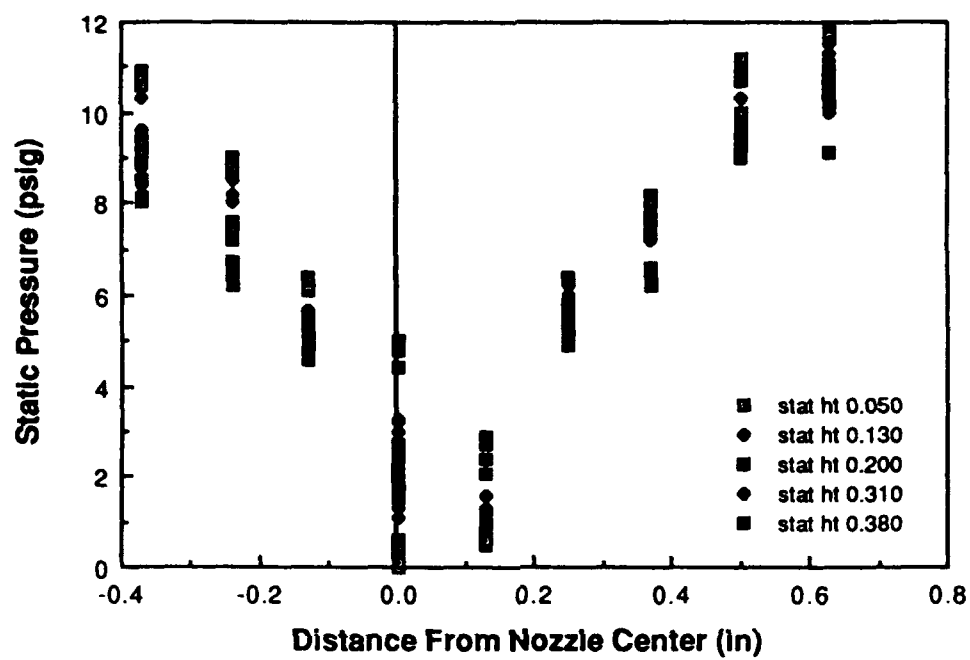**Figure 12a Static Pressure Versus the Radial Distance**
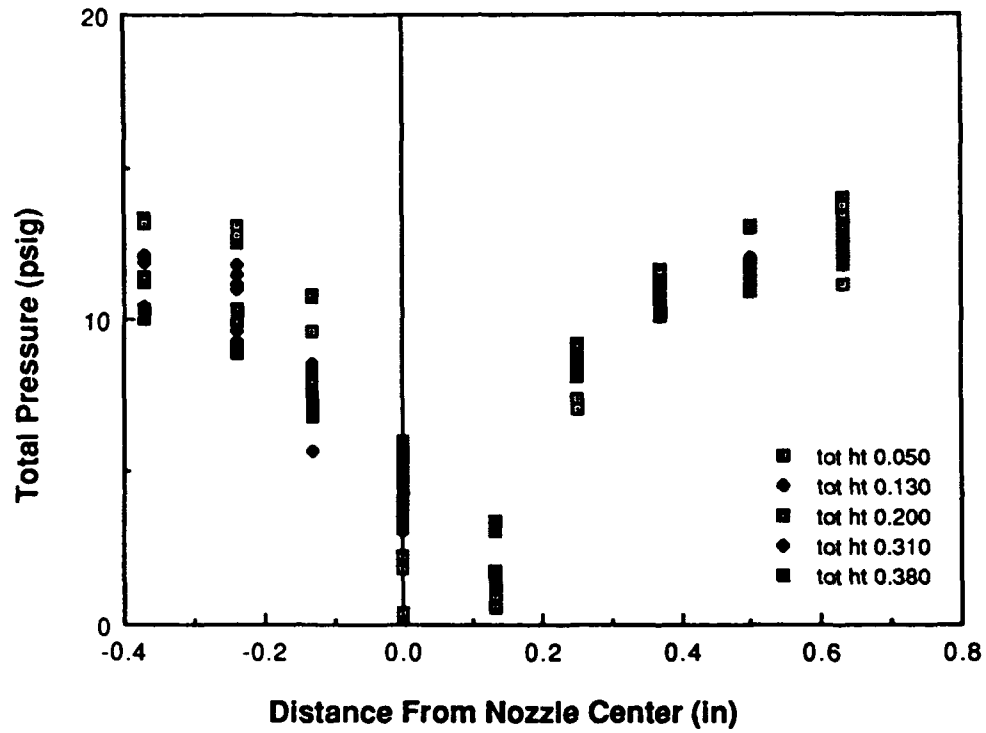Offset of 0.350 in
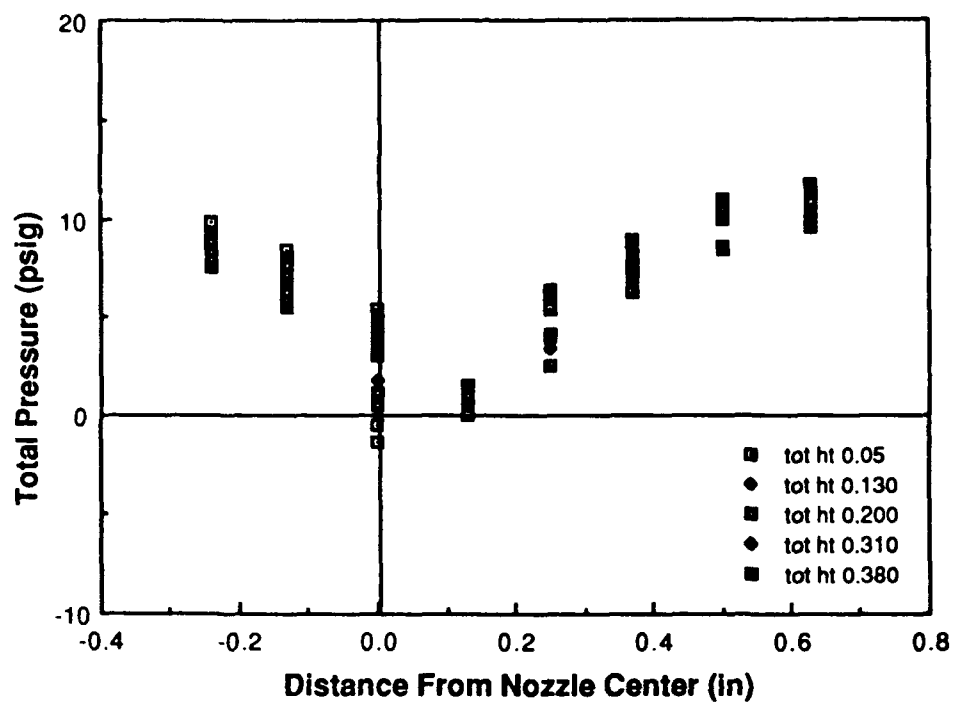
Figure 12b Total Pressure Versus the Radial Distance
Offset of 0.350 in
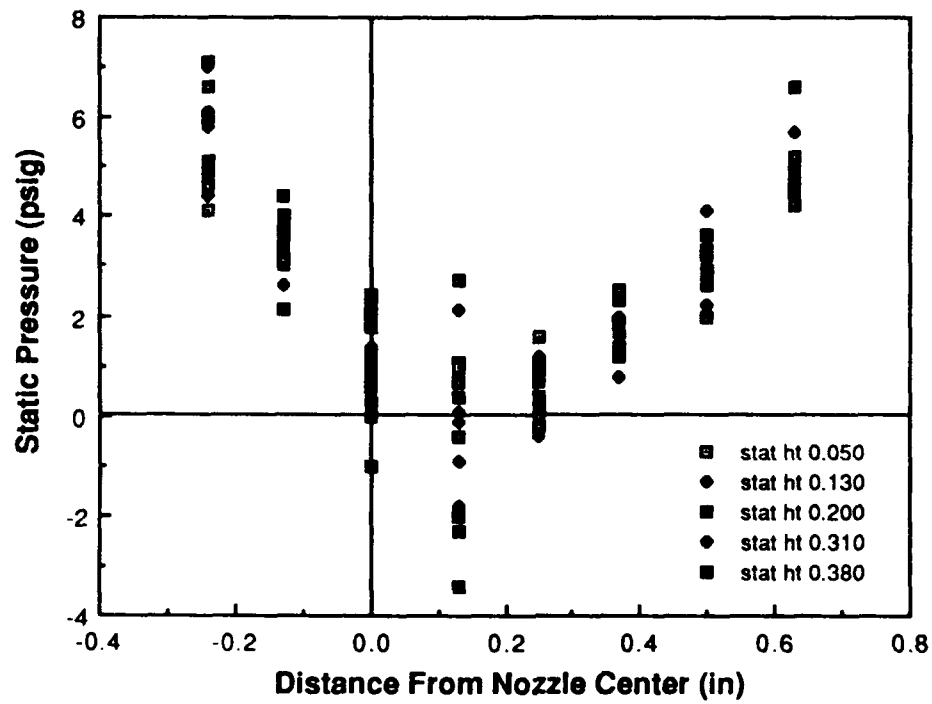
Figure 13a Static Pressure Versus the Radial Distance
Offset of 0.390 In
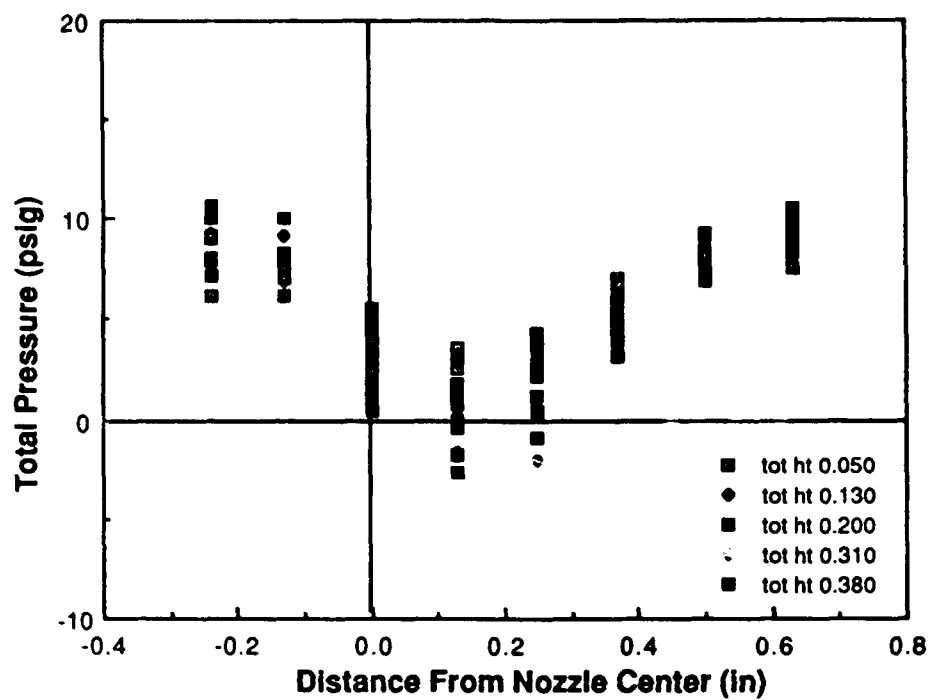
Figure 13b Total Pressure Versus the RAdial Distance
Offset of 0.390 In

Calculating the disturbing force requires the following considerations: the measured mass flow rate must equal the mass of the gas flowing through the exit nozzle; and, in the vortex cavity, there is a limiting streamline below which the flowing nitrogen will pass through and out of the nozzle and above which will recirculate back into the cavity. The mass flow out of the nozzle is a function of this streamline given as:

$$\dot{m} = \int_0^h rV\, d\mathcal{A} \tag{8}$$

By using :

$$d\mathcal{A} = w\, dh \tag{9}$$

with w set equal to the diameter of the nozzle, equation (7) simplifies to:

$$\dot{m} = w \int_0^h rV\, dh \tag{10}$$

To find this effective height, the measured mass flow rate and equation (10) are set equal. The calculated force becomes:

$$F_S = w \int_0^{h_{eff}} rV^2\, dh \tag{11}$$

A comparison of the calculated side force to the measured side force tested the simplified model and revealed that the calculation was over-simplified. This is due to the unknown pressure distribution on the outer edge of the limiting streamline Figure 21. Therefore, the disturbing force is the difference of the momentum on opposing sides of the nozzle on the same circumferential line of the vortex, Figure 22. Appendix A shows the total and static pressures at these locations. The calculated force is:

$$F_S = \left[w \int_0^h \rho V^2\, dh + \int_0^{\mathcal{A}} p\, d\mathcal{A} \right]_{1^{st}\text{side}} - \left[w \int_0^h \rho V^2\, dh + \int_0^{\mathcal{A}} p\, d\mathcal{A} \right]_{2^{nd}\text{side}} \tag{12}$$

Given the similarity of the results of this calculated side force and the measured side force, as evidenced in Appendix C, the primary dependent variable is the magnitude of the tangential velocity of the gas at the nozzle. Figure 23 shows the comparison between the calculated force and the measured force.
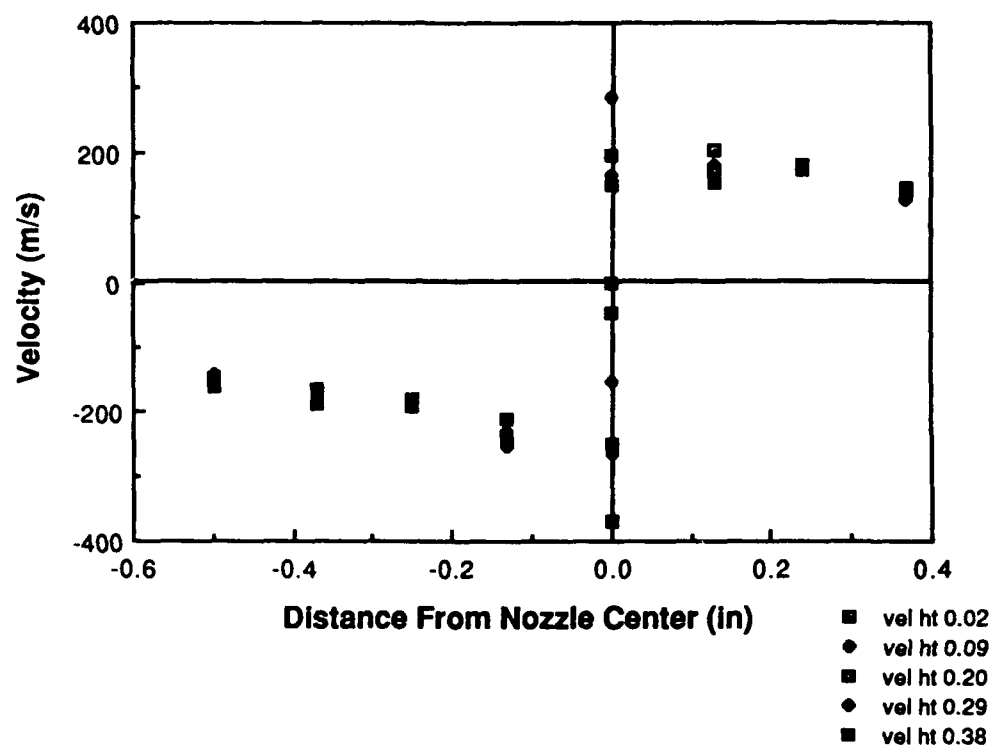
Figure 14   Velocity Profile Coincident Centers

24
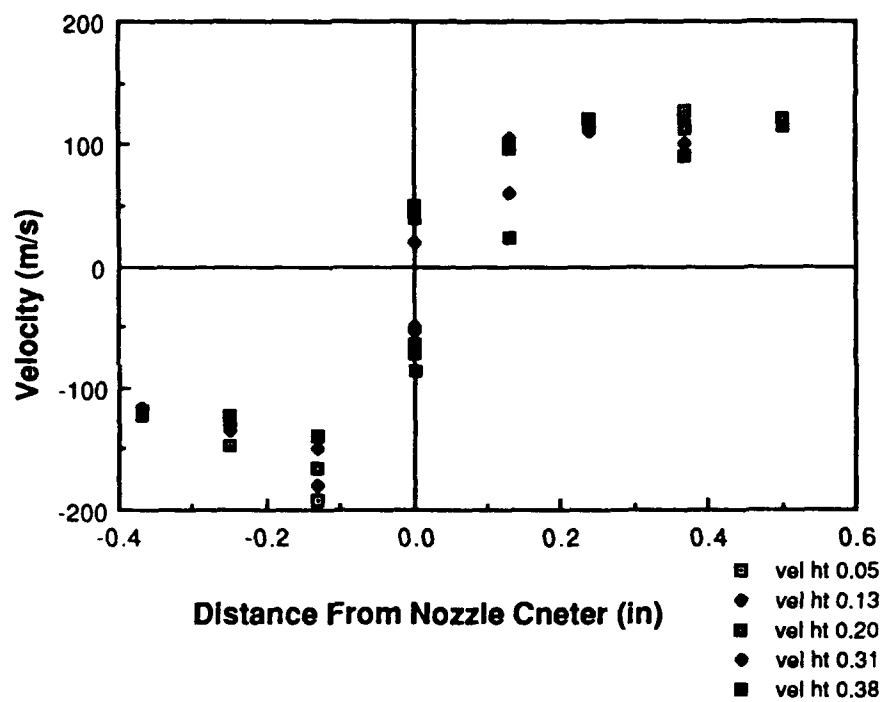
Figure 15 Velocity Profile Offset of 0.210 in
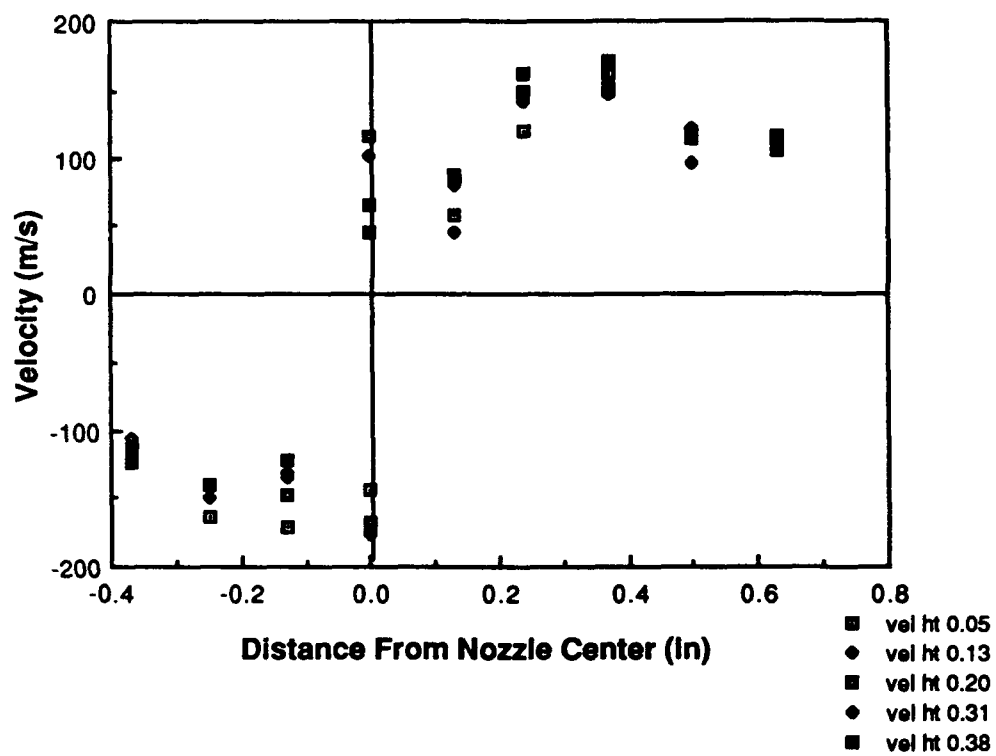
Figure 16 Velocity Profile Offset 0.250 in
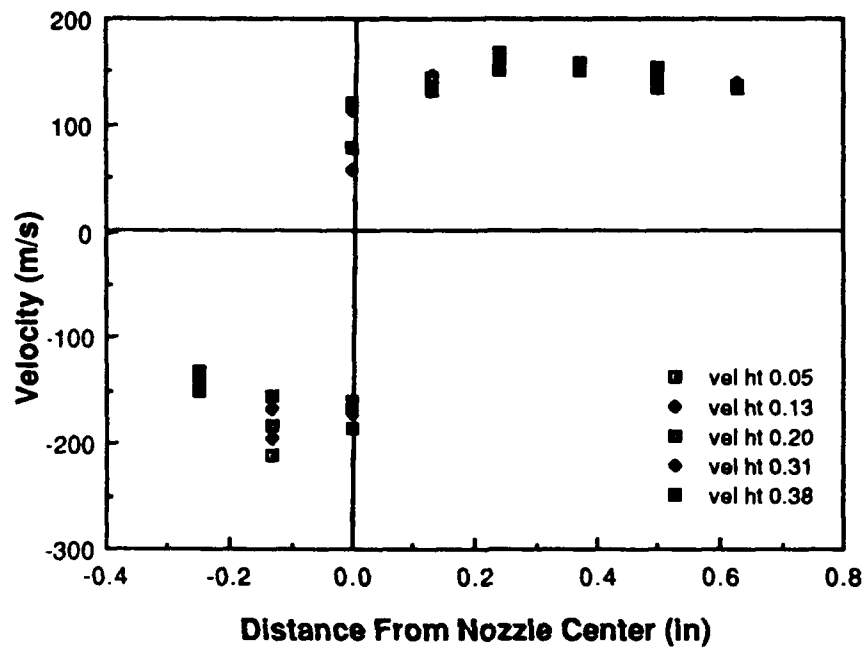
Figure 17 Velocity Profile Offset of 0.300 In
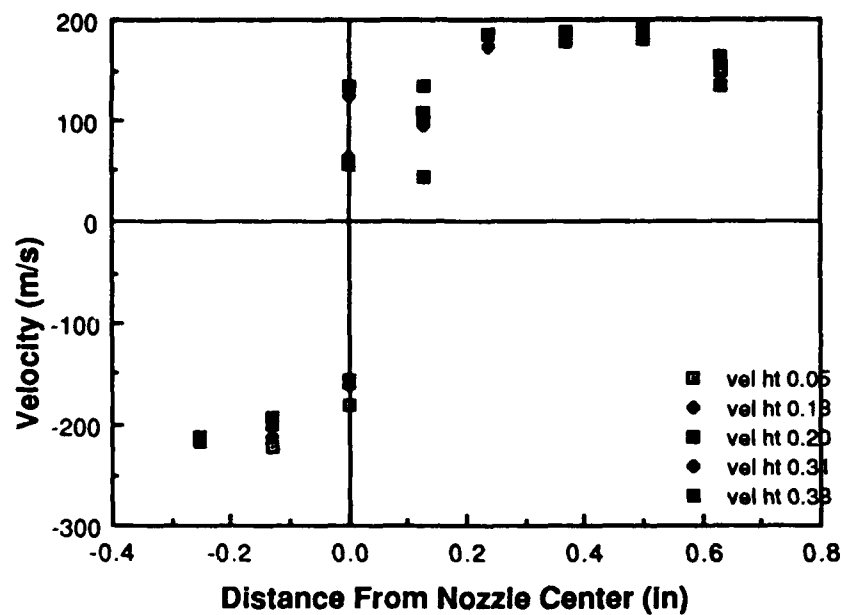
figure 18 Velocity Profile offset of 0.350 in
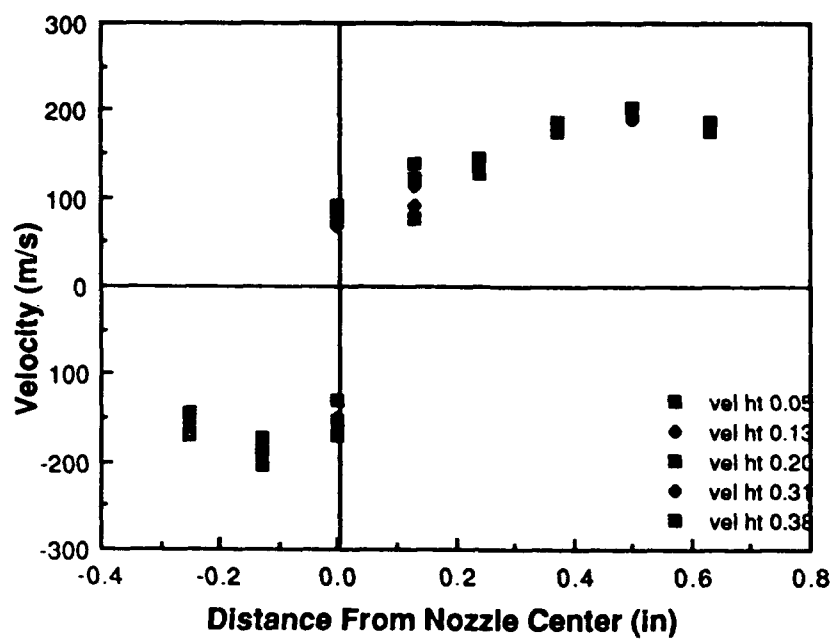
Figure 19   Velocity Profile Offset of 0.390 in
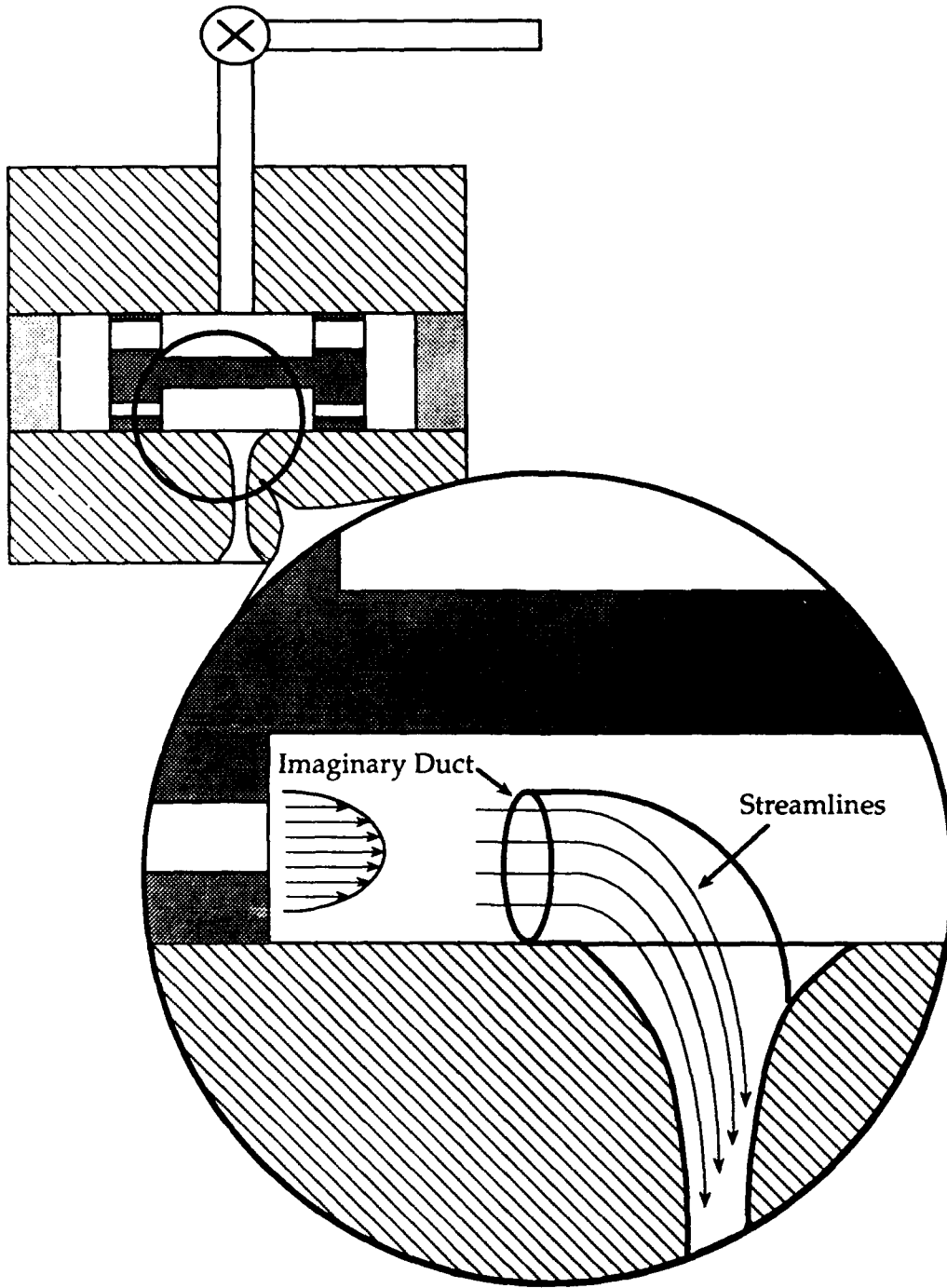
FIGURE 20

IMAGINARY DUCT AND STREAMLINES
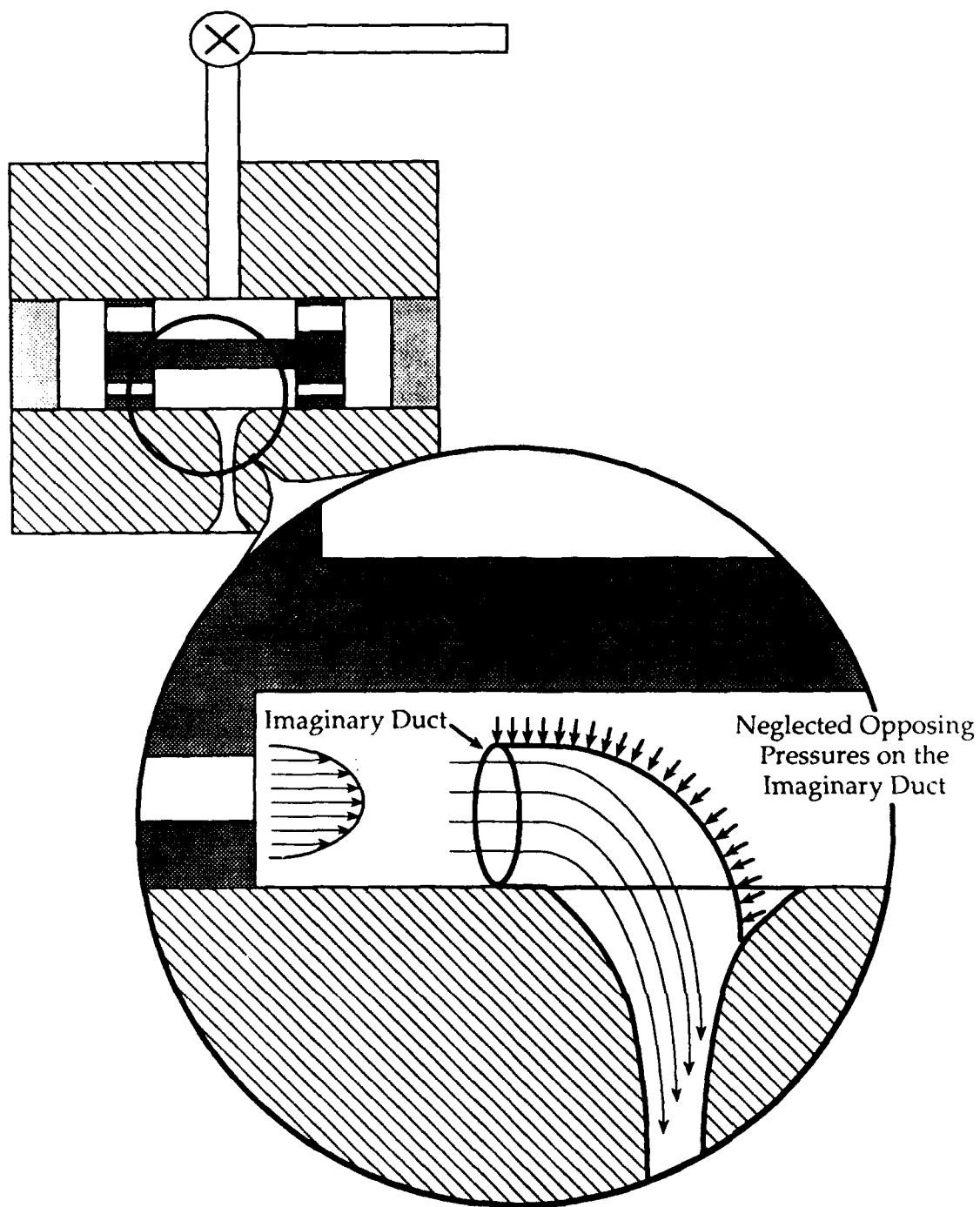
FIGURE 21

NEGLECTED OPPOSING PRESSURES ON THE

IMAGINARY DUCT
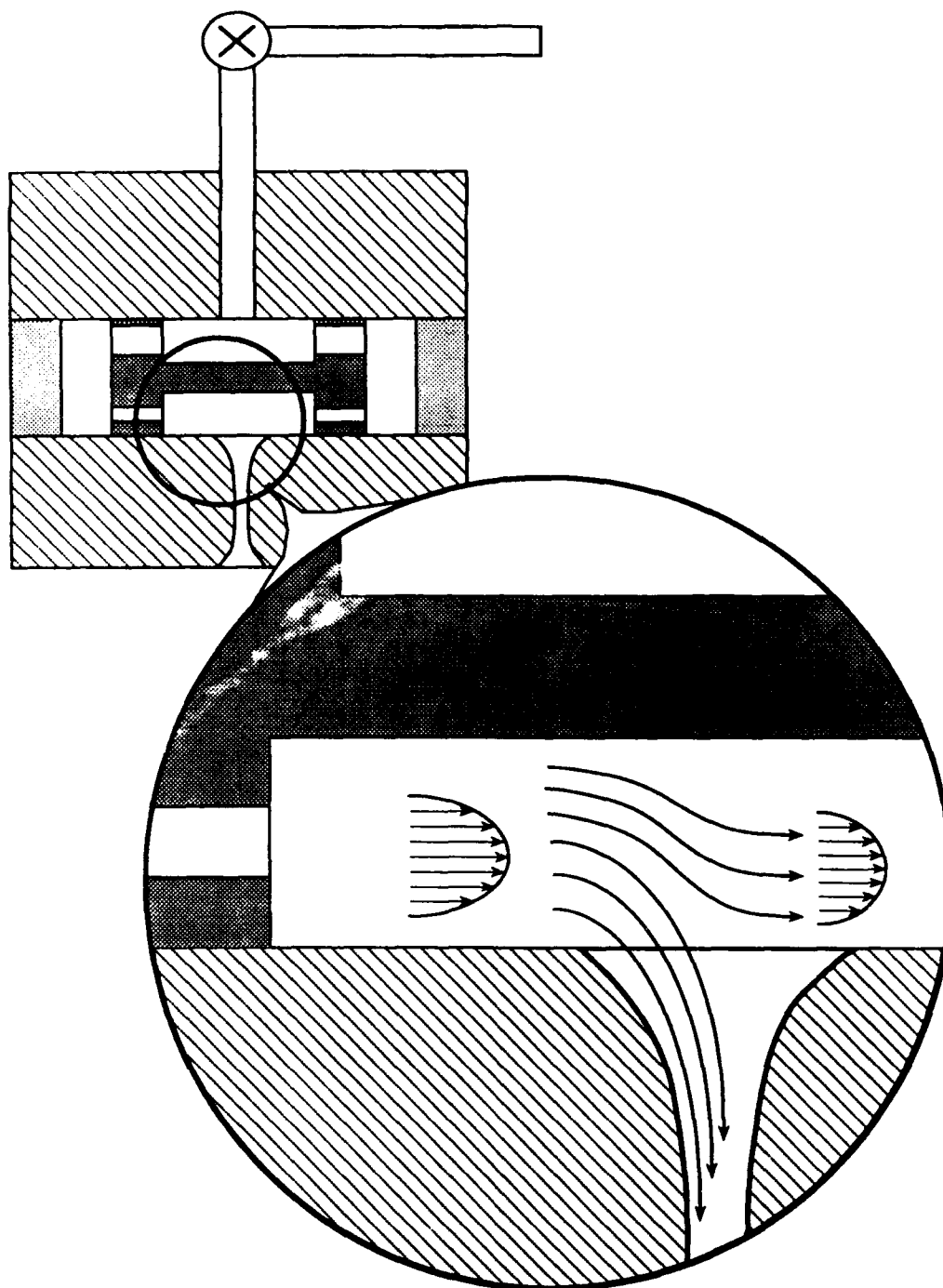
FIGURE 22

DIFFERENCE OF MOMENTUM ON OPPOSING SIDES
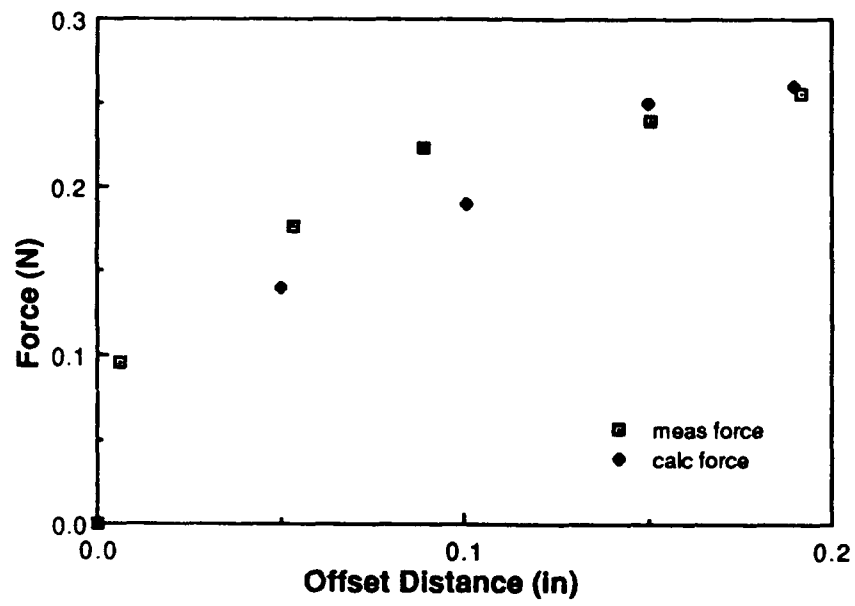
OF THE NOZZLE

Figure 23 Measured and Calculated Force

CONCLUSIONS

1. For every configuration tested, a misalignment of the center of the vortex and the center of the nozzle resulted in a steady force exerted on the nozzle at a right angle to a line connecting the center of the vortex and the center of the nozzle and in the direction directed by the tangential velocity.

2. The magnitude of the produced force can be accurately predicted from simple momentum consideration. Summation at the entrance of the nozzle indicates that the force derives from turning the tangential flow 90 degrees to exit the nozzle (Appendix C and Figure 21).

3. The primary dependent variable seems to be the magnitude of the tangential velocity of the gas at the exit nozzle.

4. Preliminary tests to simulate a submerged nozzle show the submerged nozzle does not appreciatively change the side force magnitude or the direction (Figure 7).

5. Cursory tests done to simulate a contoured aft end indicate that the side force magnitude can be dramatically reduced--but not eliminated--by contouring the aft end. The assumption is that the contouring causes the vortex to become more aligned with the nozzle center line, therefore reducing the tangential velocity vector at the entrance to the nozzle (Figure 7).

6. The implication for larger scale devices is that :

a. The coning motion may create vortices which are misaligned with the nozzle. These vortices modify the tangential velocity profile (Figure's 16-21) at the entrance to the nozzle which causes the observed force.

b. The tangential velocity profile at the entrance to the nozzle can be changed by a modification of the nozzle entrance contours.

APPENDIX A

Average values for the measured **Total** and **Static Pressures** at various locations and radial distances may be found on the following 5 pages

Average pressures at *Nozzle Offset* of: 0.210 Inches

Radial Distance (Inches)	Probe Height (Inches)	Static Pressure (psig)	Standard Deviation	Total Pressure (psig)	Standard Deviation
-0.370	0.050	11.3	0.07	13.7	0.08
-0.370	0.130	10.6	0.18	12.7	0.23
-0.370	0.200	9.9	0.16	12.1	0.13
-0.370	0.310	9.3	0.26	11.3	0.09
-0.370	0.380	8.4	0.28	10.4	0.15
-0.240	0.050	7.7	0.13	10.8	0.42
-0.240	0.130	7.4	0.05	9.9	0.45
-0.240	0.200	6.8	0.11	9.1	0.46
-0.240	0.310	6.3	0.05	8.5	0.38
-0.240	0.380	6.0	0.05	7.9	0.24
-0.130	0.050	3.9	0.26	8.5	0.31
-0.130	0.130	3.8	0.15	7.7	0.31
-0.130	0.200	3.6	0.13	6.8	0.32
-0.130	0.310	3.5	0.17	6.1	0.12
-0.130	0.310	3.6	0.11	5.8	0.11
0.000	0.050	1.3	0.34	2.0	0.72
0.000	0.130	0.9	0.48	1.2	0.68
0.000	0.200	1.3	0.17	1.7	0.62
0.000	0.310	1.0	0.43	1.2	0.45
0.000	0.380	1.5	0.40	2.0	0.47
0.000	0.050	-0.5	0.00	-0.3	0.11
0.000	0.130	0.1	0.00	0.1	0.04
0.000	0.200	0.1	0.04	0.4	0.05
0.000	0.310	-0.4	0.22	-0.2	0.11
0.000	0.380	0.8	0.05	1.0	0.11
0.130	0.050	0.4	0.19	1.3	0.09
0.130	0.130	0.5	0.15	1.5	0.15
0.130	0.200	0.6	0.11	1.4	0.17
0.130	0.310	0.3	0.11	0.6	0.19
0.130	0.380	0.7	0.05	0.7	0.07
0.250	0.050	2.7	0.08	4.1	0.08
0.250	0.130	2.9	0.08	4.3	0.12
0.250	0.200	2.9	0.08	4.4	0.12
0.250	0.310	2.6	0.05	3.9	0.11
0.250	0.380	2.3	0.07	3.8	0.09
0.370	0.050	3.5	0.29	5.3	0.05
0.370	0.130	3.6	0.31	5.2	0.04
0.370	0.200	3.6	0.36	5.0	0.04
0.370	0.310	3.5	0.32	4.6	0.05
0.370	0.380	3.6	0.23	4.5	0.08
0.500	0.050	5.0	0.08	6.6	0.24
0.500	0.130	4.8	0.07	6.4	0.18
0.500	0.200	4.4	0.13	6.1	0.08
0.500	0.310	4.3	0.10	5.8	0.16
0.500	0.380	4.3	0.07	5.8	0.12

Average pressures at *Nozzle Offset* of: 0.250 Inches

Radial Distance (Inches)	Probe Height (Inches)	Static Pressure (psig)	Standard Deviation	Total Pressure (psig)	Standard Deviation
-0.370	0.050	10.8	0.11	13.2	0.04
-0.370	0.130	9.8	0.32	12.0	0.08
-0.370	0.200	9.1	0.14	11.1	0.40
-0.370	0.310	8.8	0.38	10.4	0.05
-0.370	0.380	8.3	0.23	10.1	0.07
-0.240	0.050	8.8	0.14	12.8	0.21
-0.240	0.130	8.2	0.18	11.4	0.32
-0.240	0.200	7.4	0.15	10.1	0.14
-0.240	0.310	6.6	0.11	9.3	0.16
-0.240	0.380	6.4	0.18	9.0	0.08
-0.130	0.050	6.0	0.42	9.9	1.01
-0.130	0.130	5.5	0.15	7.6	1.10
-0.130	0.200	4.8	0.19	7.5	0.34
-0.130	0.310	5.0	0.15	7.2	0.23
-0.130	0.310	5.3	0.11	7.1	0.25
0.000	0.050	0.5	0.11	2.5	0.52
0.000	0.130	1.2	0.10	4.2	0.22
0.000	0.200	1.7	0.11	4.7	0.36
0.000	0.310	2.1	0.22	5.5	0.50
0.000	0.380	2.5	0.18	5.8	0.11
0.000	0.050	0.1	0.07	0.3	0.08
0.000	0.130	1.9	0.27	3.3	0.11
0.000	0.200	2.0	0.13	3.4	0.18
0.000	0.310	3.2	0.11	4.3	0.21
0.000	0.380	4.7	0.26	5.2	0.11
0.130	0.050	0.6	0.11	0.9	0.17
0.130	0.130	1.3	0.22	1.5	0.21
0.130	0.200	1.0	0.04	1.7	0.04
0.130	0.310	1.0	0.17	1.6	0.15
0.130	0.380	2.5	0.30	3.3	0.13
0.250	0.050	5.5	0.16	7.3	0.13
0.250	0.130	6.1	0.09	8.7	0.15
0.250	0.200	6.1	0.30	9.0	0.13
0.250	0.310	5.8	0.12	8.5	0.22
0.250	0.380	5.1	0.15	8.4	0.25
0.370	0.050	7.6	0.35	11.3	0.25
0.370	0.130	7.7	0.36	10.8	0.11
0.370	0.200	7.7	0.16	10.9	0.08
0.370	0.310	7.5	0.20	10.9	0.15
0.370	0.380	6.4	0.15	10.4	0.19
0.500	0.050	11.0	0.18	13.1	0.05
0.500	0.130	10.5	0.34	11.9	0.04
0.500	0.200	9.7	0.16	11.8	0.08
0.500	0.310	9.3	0.19	11.5	0.16
0.500	0.380	9.1	0.11	11.0	0.07
0.630	0.050	11.7	0.40	13.6	0.29
0.630	0.130	11.2	0.19	13.0	0.18
0.630	0.200	10.7	0.27	12.8	0.18
0.630	0.310	10.4	0.22	12.4	0.15
0.630	0.380	10.4	0.12	12.1	0.22

Average pressures at *Nozzle Offset* of: **0.300 Inches**

Radial Distance (Inches)	Probe Height (Inches)	Static Pressure (psig)	Standard Deviation	Total Pressure (psig)	Standard Deviation
-0.240	0.050	7.6	0.78	10.7	0.69
-0.240	0.130	7.2	0.75	10.3	0.64
-0.240	0.200	6.7	0.68	9.4	0.52
-0.240	0.310	6.2	0.66	8.7	0.53
-0.240	0.380	5.9	0.57	8.1	0.57
-0.130	0.050	3.6	0.12	9.3	0.48
-0.130	0.130	3.9	0.49	8.7	0.33
-0.130	0.200	3.6	0.48	7.7	0.57
-0.130	0.310	3.8	0.49	7.1	0.52
-0.130	0.380	3.9	0.58	6.7	0.45
0.000	0.050	0.7	0.54	4.3	0.24
0.000	0.130	1.5	0.22	4.6	0.16
0.000	0.200	1.8	0.37	4.5	0.22
0.000	0.310	2.2	0.52	5.2	0.53
0.000	0.310	2.3	0.79	5.3	0.45
0.000	0.050	-0.9	0.24	-0.4	0.12
0.000	0.130	0.6	0.12	0.9	0.42
0.000	0.200	0.5	0.00	1.1	0.24
0.000	0.310	0.4	0.14	1.6	1.40
0.000	0.380	1.5	0.17	3.0	1.70
0.130	0.050	0.7	0.33	2.7	0.83
0.130	0.130	0.8	0.37	2.9	0.82
0.130	0.200	0.9	0.24	2.9	0.83
0.130	0.310	1.3	0.41	3.0	1.50
0.130	0.380	2.0	0.42	3.8	1.10
0.250	0.050	4.4	0.50	7.9	0.37
0.250	0.130	4.9	0.41	8.1	0.29
0.250	0.200	5.1	0.45	8.0	0.17
0.250	0.310	5.1	0.54	8.0	0.24
0.250	0.380	4.9	0.66	7.8	0.14
0.370	0.050	6.3	0.58	9.7	0.37
0.370	0.130	6.4	0.63	9.7	0.26
0.370	0.200	6.3	0.50	9.6	0.31
0.370	0.310	6.3	0.42	9.3	0.40
0.370	0.380	6.2	0.25	9.2	0.75
0.500	0.050	6.6	0.65	9.0	1.60
0.500	0.130	6.3	0.53	8.7	1.20
0.500	0.200	5.9	0.29	8.5	1.10
0.500	0.310	5.8	0.50	8.4	1.10
0.500	0.380	5.4	0.12	8.4	0.94
0.630	0.050	7.1	0.41	9.7	1.30
0.630	0.130	7.0	0.57	9.5	1.30
0.630	0.200	6.8	0.62	9.2	0.98
0.630	0.310	6.6	0.57	9.2	0.91
0.630	0.380	6.6	0.33	9.1	0.87

Average pressures at *Nozzle Offset* of: 0.350 Inches

Radial Distance (Inches)	Probe Height (Inches)	Static Pressure (psig)	Standard Deviation	Total Pressure (psig)	Standard Deviation
-0.240	0.050	3.5	0.25	9.4	0.26
-0.240	0.130	3.1	0.38	9.0	0.16
-0.240	0.200	2.9	0.36	8.7	0.25
-0.240	0.310	2.7	0.19	8.3	0.21
-0.240	0.380	2.4	0.29	7.8	0.24
-0.130	0.050	2.6	0.31	8.7	0.13
-0.130	0.130	2.6	0.33	8.0	0.98
-0.130	0.200	2.7	0.45	7.5	0.91
-0.130	0.310	2.5	0.40	7.1	0.90
-0.130	0.380	2.4	0.28	6.7	0.86
0.000	0.050	1.5	0.56	5.0	0.26
0.000	0.130	1.4	0.68	4.1	0.21
0.000	0.200	1.7	0.66	4.3	0.52
0.000	0.310	2.0	0.45	4.7	0.24
0.000	0.310	2.1	0.45	4.8	0.37
0.000	0.050	-0.9	0.42	-0.7	0.42
0.000	0.130	0.2	0.05	0.6	0.22
0.000	0.200	0.4	0.24	0.7	0.39
0.000	0.310	0.8	0.17	2.3	0.62
0.000	0.380	1.6	0.05	3.4	0.59
0.130	0.050	-0.6	0.31	1.0	0.64
0.130	0.130	0.2	0.09	1.0	0.43
0.130	0.200	0.1	0.09	1.1	0.66
0.130	0.310	0.3	0.12	1.2	0.43
0.130	0.380	0.9	0.45	1.1	0.52
0.250	0.050	1.2	0.46	3.8	1.20
0.250	0.130	1.4	0.41	4.6	1.00
0.250	0.200	1.5	0.42	5.2	0.88
0.250	0.310	1.4	0.54	5.1	0.94
0.250	0.380	1.4	0.59	5.1	0.99
0.370	0.050	3.4	0.43	7.1	0.93
0.370	0.130	3.7	0.29	7.5	0.67
0.370	0.200	3.8	0.40	8.1	0.51
0.370	0.310	3.9	0.46	8.2	0.54
0.370	0.380	3.8	0.62	7.8	0.85
0.500	0.050	4.8	0.50	9.4	1.20
0.500	0.130	5.0	0.68	9.2	1.10
0.500	0.200	4.9	0.57	9.1	0.90
0.500	0.310	4.7	0.41	8.9	0.68
0.500	0.380	4.3	0.50	8.9	0.73
0.630	0.050	7.7	0.88	11.5	0.21
0.630	0.130	7.6	0.83	11.0	0.24
0.630	0.200	7.6	0.76	10.7	0.12
0.630	0.310	7.5	0.99	10.1	0.08
0.630	0.380	7.3	0.97	9.7	0.05

Average pressures at *Nozzle Offset* of: 0.390 Inches

Radial Distance (Inches)	Probe Height (Inches)	Static Pressure (psig)	Standard Deviation	Total Pressure (psig)	Standard Deviation
-0.240	0.050	4.9	0.74	7.4	0.81
-0.240	0.130	5.1	0.73	8.2	0.87
-0.240	0.200	5.4	0.85	9.1	0.90
-0.240	0.310	5.9	0.86	9.5	1.04
-0.240	0.380	6.0	0.86	9.8	1.18
-0.130	0.050	3.6	0.60	6.7	0.66
-0.130	0.130	3.5	0.29	7.2	0.31
-0.130	0.200	3.3	0.28	7.5	0.37
-0.130	0.310	3.2	0.54	8.3	0.70
-0.130	0.380	3.2	0.82	8.8	0.88
0.000	0.050	1.8	0.38	3.5	0.38
0.000	0.130	1.3	0.62	3.6	0.37
0.000	0.200	1.2	0.45	3.6	0.90
0.000	0.310	1.0	0.73	3.7	1.30
0.000	0.310	1.1	0.65	4.1	1.67
0.000	0.050	2.2	0.12	2.8	0.41
0.000	0.130	1.9	0.34	2.4	0.41
0.000	0.200	1.3	0.50	1.9	0.49
0.000	0.310	0.5	0.05	0.9	0.33
0.000	0.380	-0.2	0.56	0.6	0.62
0.130	0.050	1.6	0.78	3.1	0.41
0.130	0.130	0.9	0.90	2.1	1.08
0.130	0.200	0.2	0.45	0.8	0.90
0.130	0.310	-0.9	0.78	0.0	1.28
0.130	0.380	-2.6	0.60	-1.1	1.64
0.250	0.050	0.8	0.58	2.4	1.48
0.250	0.130	0.3	0.66	2.0	2.85
0.250	0.200	0.4	0.53	2.4	2.32
0.250	0.310	0.5	0.39	2.1	1.38
0.250	0.380	0.6	0.31	2.1	0.66
0.370	0.050	1.7	0.45	5.0	1.61
0.370	0.130	1.5	0.52	5.3	1.15
0.370	0.200	1.9	0.53	5.8	0.68
0.370	0.310	1.7	0.21	5.3	0.78
0.370	0.380	1.4	0.21	5.0	0.90
0.500	0.050	2.7	0.66	7.0	0.77
0.500	0.130	2.6	0.31	7.4	0.41
0.500	0.200	2.9	0.21	7.5	0.50
0.500	0.310	3.5	0.49	7.8	0.82
0.500	0.380	3.1	0.17	8.0	0.91
0.630	0.050	4.4	0.12	8.6	0.31
0.630	0.130	4.8	0.21	8.8	0.39
0.630	0.200	5.1	0.09	9.1	0.40
0.630	0.310	5.2	0.40	9.4	0.56
0.630	0.380	5.3	0.95	10.0	0.40

APPENDIX B

Configuration Number	Offset Distance (Centimeters)	Deflection (Centimeters)	Model Configuration
1	0.000	0.000	Original Model
2	0.000	0.000	Extended Chamber Model
3	0.000	0.000	Original with Nozzle Insert
4	0.000	0.000	Original with Clay Contour
5	0.010	0.100	Original Model
6	0.053	0.180	Original Model
7	0.090	0.220	Original Model
8	0.150	0.240	Original Model
9	0.190	0.260	Original Model
10	0.190	0.240	Extended Chamber Model
11	0.190	0.210	Original with Nozzle Insert
12	0.190	0.060	Symmetric Clay Contour
13	0.190	0.050	Asymmetric Clay Contour

APPENDIX C

Configuration Number	Offset Distance (Centimeters)	Measured Force (Newtons)	Calculated Force (Newtons)
1	0.000	0.000	0.000
2	0.006	0.096	
3	0.050		0.140
4	0.053	0.176	
5	0.089	0.224	
6	0.100		0.190
7	0.150		0.250
8	0.151	0.240	
9	0.190		0.260
10	0.192	0.256	